JOURNAL OF MATERIALS SCIENCE 25 (1990) 1407–1415

XPS investigation on AISI 420 stainless steel corrosion in oil and gas well environments

G. FIERRO, G. M. INGO*, F. MANCIA, L. SCOPPIO, N. ZACCHETTI
Centro Sviluppo Materiali SpA, P. O. Box 10747 00100 ROMA-EUR (Italy)

The corrosion behaviour of 13Cr-martensitic stainless steel (AISI 420) was investigated in CO_2–H_2S–Cl^- environments typical of oil and gas wells under different CO_2 and H_2S partial pressures. The corrosion tests indicated that the AISI 420 steel was highly corrosion resistant to CO_2-induced phenomena (general corrosion and carbonate S.C.C.), while in the H_2S environment a high S.S.C.C. (Sulphide Stress Corrosion Cracking) susceptibility and high corrosion rates were found. Moreover, CO_2 in CO_2–H_2S–Cl^- systems inhibited general corrosion and S.S.C.C. phenomena by favouring the formation of a protective film. By means of X-ray photoelectron spectroscopy (XPS) the chemical nature of the films grown on AISI 420 in different environmental conditions was investigated and the following statements were drawn out:

– CO_2 favours the growth of a hydrated Cr-oxide rich protective film with a low Fe-oxide and sulphide content;

– the presence of H_2S favours the formation of less protective Fe-sulphide and Fe-oxide rich layers.

Furthermore from XPS results an index of protectiveness $I_p = Cr^{+3}/(Cr^{+3} + Fe^{ox})$ was defined and related to the environmental parameter $E_{H_2S,CO_2} = pCO_2/pH_2S + pCO_2$ and to the corrosion rates.

1. Introduction

The use limits of 13Cr-martensitic stainless steel (AISI 420) in gas and oil wells (CO_2–H_2S–Cl^- in aqueous solution, T = 80–120° C) are difficult to determine due to the presence of different failure phenomena depending on the environmental variables (partial pressures, temperatures, pH, chloride content) [1–5].

The technological characterizations carried out so far, in autoclaves simulating operating conditions, have revealed [6–9] a high suspectibility of 13Cr stainless steel to cracking induced by H_2S aqueous system, Sulphide Stress Corrosion Cracking, (S.S.C.C.), Hydrogen Induced Cracking (H.I.C), and a good corrosion resistance in CO_2 aqueous system due to the inhibiting effect of CO_2 on the corrosion rate [10].

Moreover Stress Corrosion Cracking (S.C.C.) tests carried out in CO_2–H_2S aqueous systems showed that the σ_{th} (stress-threshold for SSC onset) values obtained are higher than the typical values obtained in H_2S systems.

These corrosion phenomena have been explained by the growth of protective films [5, 7, 11, 12], but only in a few cases has the nature of these films been investigated and chromium carbonates, complex mixture of iron – chromium sulphide and carbonates have been determined [12, 13]. Moreover published data on iron–25Cr alloy exposed to H_2S atmospheres (up to 300° C) indicate the growth of FeS and Fe–Cr oxide layers [14, 15].

The aim of this work is to establish by means of X-ray Photoelectron Spectroscopy (XPS) the chemical composition of the films grown on AISI 420 in H_2S–CO_2–Cl^- aqueous environments in a wide range of pH_2S and pCO_2 partial pressures, with a NaCl content of 50 gl^{-1}, pH = 2.7 and 4.8, T = 80° C, to relate the corrosion data with the nature of these complex films.

2. Experimental details

The photoelectron spectra were performed with a Leybold & Heraeus LHS10 spectrometer equipped with an EA11 electron analyser, using an unmonochromatized $AlK\alpha_{1,2}$ ($h\nu$ = 1 486.6 eV) radiation.

The electron analyser operated in FAT mode selecting a constant pass energy of 50 eV. Under such conditions the Full Width at Half Maximum (FWHM) of $Ag_{3d5/2}$ peak of an Ar^+ sputtered silver metal surface was 1.01 eV. All measurements were performed at pressures lower than 10^{-10} mbar in the analysis chamber.

The samples were in Ohmic contact with the electron spectrometer.

The Binding Energies (B.E.) were referenced to the

Present address: CNR, Istituto di Teoria e Struttura Elettronica, P.O. Box 10, 00016 Monterotondo Stazione, Roma.

0022–2461/90 $03.00 + .12

TABLE I Chemical analysis of the 13Cr steel (AISI 420)

C	Cr	Ni	Mn	Mo	P	S	Si	Cu	Al	Co
0.22	13.23	–	0.48	0.03	0.014	0.002	0.39	0.027	0.08	0.018

Thermal treatments
- Austenitization 920° C, water quenching
- Tempering 620° C - 1 h.

Fermi level of the electron analyser and the B.E. scale was calibrated against the $Au_{4f7/2}$ and $Cu_{2p3/2}$ peaks at 83.8 eV and 932.5 eV respectively.

The correction of the binding energy shifts due to surface charging was made by referring to the C_{1s} line of adsorbed hydrocarbons (284.5 eV) and $Ar_{2p3/2}$ line of implanted Ar^+ ions (242.2 eV). Core level electron binding energies were reproducible within $\pm$ 0.2 eV.

The samples were sputtered with a Leybold & Heraeus 12Q63 scanning ion gun operating, unless otherwise stated, with 2 KeV argon ion energy (current density $J_p = 3.4\,\mu A\,cm^{-2}$, argon pressure 5×10^{-5} mbar, scanned area 10×10 mm, sputtering rate 0.4 nm $Ta_2O_5\,min^{-1}$).

The spectra were recorded and handled using a HP 2113E data system. The data handling procedure involved the following steps:

1) Smoothing with constant parameters (least squares fit with a second degree polynomial of five neighbouring experimental points);

2) inelastic background remotion by a non-linear *S* type integral background profile;

3) the quantitative analysis was determined for each sample from the peak area after smoothing and background subtraction, corrected with the sensitivity factors proposed by Wagner [16]. These latter were checked and confirmed in some reference samples (anhydrous Fe_2O_3, Cr_2O_3, CrO_3).

The chemical composition and the thermal treatments of AISI 420 in form of well casing is shown in Table I. Autoclave tests (480 h) involving exposures in H_2S–CO_2–Cl^- deaerated environments were carried out using specimens of different size for corrosion rates measurements and XPS analysis.

The environmental conditions used in the autoclave tests and the experimental corrosion rate results are shown in Table II.

3. Results and discussion

In Figs 1, 2, 3, 4, 5 are shown the most representative depth profiles obtained by means of XPS analysis combined with Ar^+ sputtering sequences.

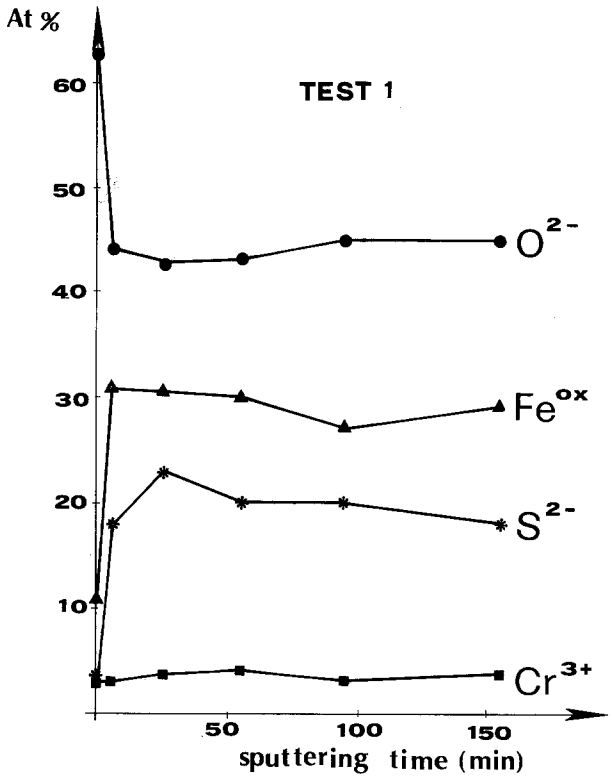

Figure 1 XPS depth profile of Test 1.

The carbon depth profile is not reported in order to outline better the profiles of the other species which are present.

The carbon due to the environmental contamination (C–O and C–H bonds, see Fig. 6) was about 30% for the as-received samples and dropped down to negligible values after the first exposure to argon ions, thus demonstrating the absence of carbonates.

XPS analysis of chromium chemical state (see Fig. 7) revealed that both hydrous and anhydrous oxides are present, as confirmed by the O_{1s} spectra. The metallic chromium is not present and even after prolonged argon sputtering it doesn't appear. Furthermore from the $Cr_{2p3/2}$ binding energy value (577 $\pm$ 0.2) we exclude the presence of chromium sulphide (574.5 $\pm$ 0.2 eV) [17].

The iron valence state on the as-received samples is Fe^{+3} as shown in Fig. 8, where the typical broad satellite peaks at higher binding energy, their parent peaks ($Fe_{2p3/2}$, $Fe_{2p1/2}$), are evident.

TABLE II Environmental conditions used in autoclave tests and experimental mean corrosion rate results

Test	pH	pH_2S (bar)	pN_2 (bar)	pCO_2 (bar)	C.R. (mm y^{-1})
1	2.7	1	–	–	2.1
2	4.8	1	–	–	0.214
3	2.7	0.1	0.9	–	1.2
4	4.8	0.1	0.9	–	0.165
5	2.7	0.1	–	0.9	0.77
6	4.8	0.1	–	0.9	0.081
7	2.7	0.5	–	0.5	1.8
8	2.7	0.4	–	9.6	0.75
9	4.8	0.4	–	9.6	0.068
10	2.7	–	–	1	0.1

NaCl = 50 g l^{-1}
T = 80° C

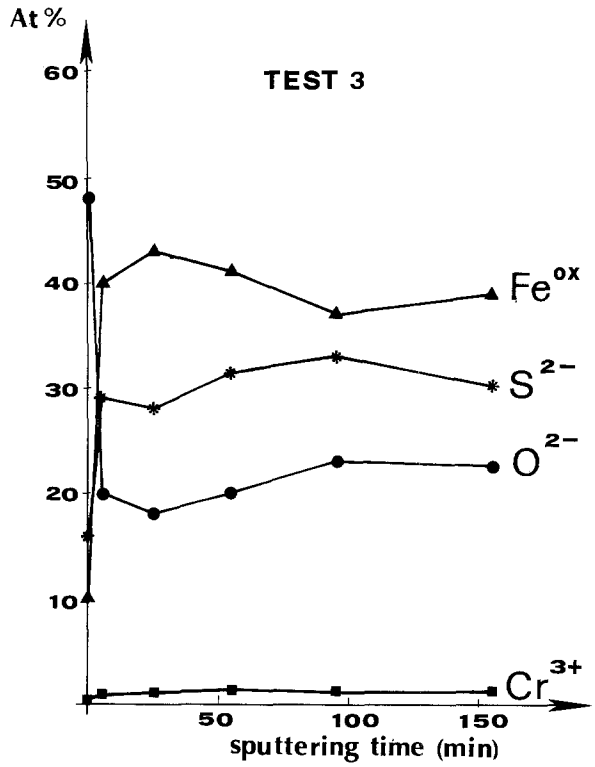

Figure 2 XPS depth profile of Test 3.

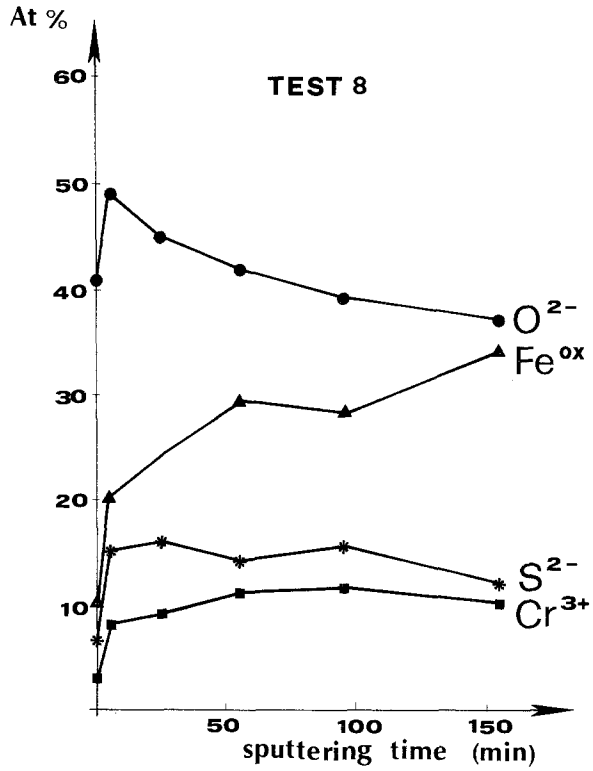

Figure 4 XPS depth profile of Test 8.

After sputtering the modified lineshape of $Fe_{2p3/2}$ suggests a partial change of the valence state to Fe^{+2}. This can be induced by argon sputtering reduction, as seen by McIntyre [18] with a higher ion current dose (3 KeV, 20 μA cm^{-2}) as against our conditions (2 KeV, 3.4 μA cm^{-2}) or more likely can be related to the growth of Fe^{+2} compounds in the corrosion film. In fact the hump in the low binding energy side of $Fe_{2p3/2}$ peak suggests the presence of Fe^{2+} [19]. Furthermore the absence of the $Fe^{3+}_{2p3/2}$ satellite can be explained by the overlapping of $Fe^{+2}_{2p1/2}$ peak with $Fe^{+3}_{2p3/2}$ and $Fe^{+2}_{2p3/2}$ satellite peaks [19]. Even though it is difficult in this case to evaluate correctly the iron chemical state due also to the large amount of coupling between the core hole created by photoemission and the high spin states of iron [20, 21, 22], we suggest on the basis of binding energy and quantitative results, values the presence in the inner layers of a mixture of both hydrous iron oxide (Fe^{+2}, Fe^{+3}) and iron sulphide.

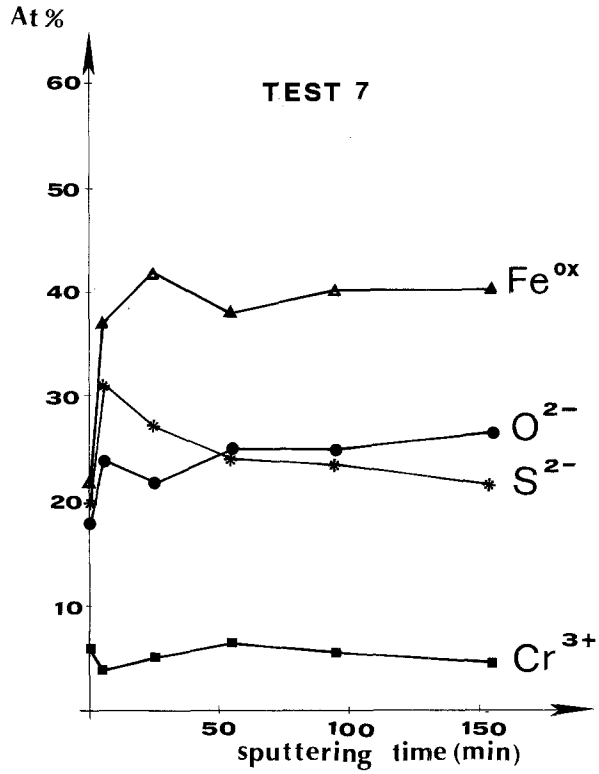

Figure 3 XPS depth profile of Test 7.

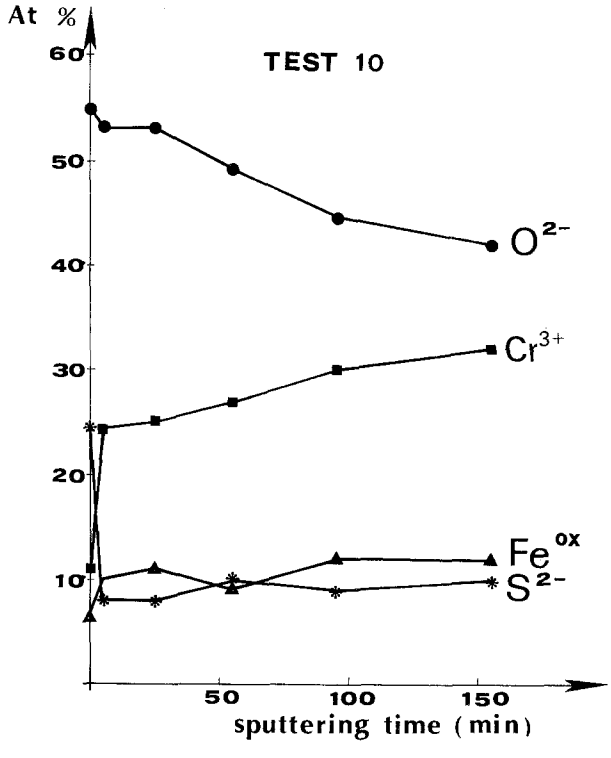

Figure 5 XPS depth profile of Test 10.

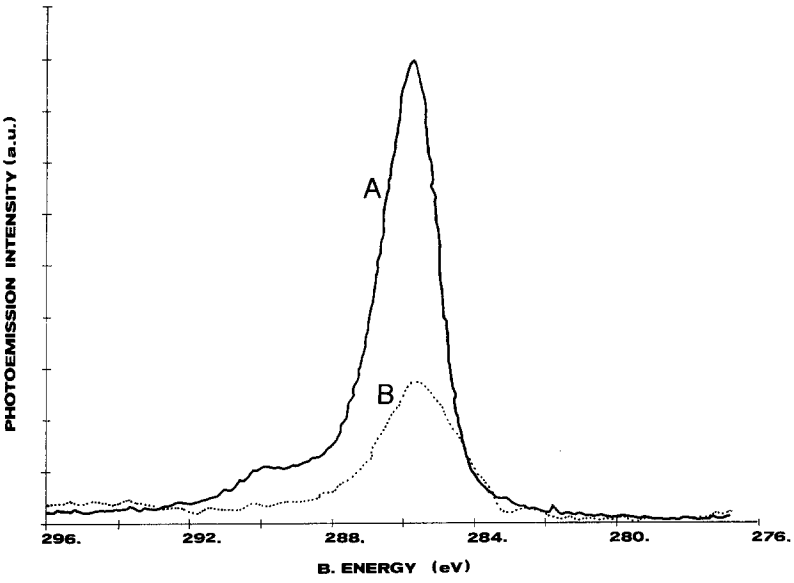

Figure 6 C_{1s} photoelectron spectra A) as received sample B) after 5 minutes of Ar^+ sputtering.

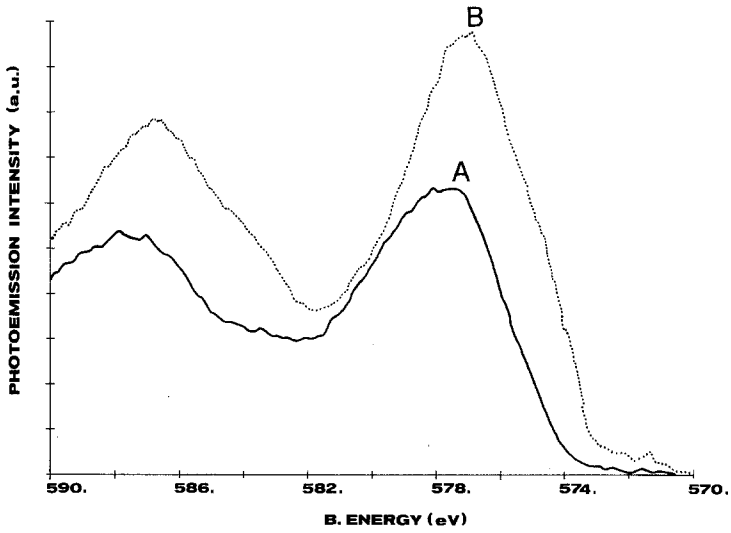

Figure 7 $Cr_{2p1/2,3/2}$ photoelectron spectra A) as received sample B) after 5 minutes of Ar^+ sputtering.

The slight chemical shift towards lower binding energies found for $Fe_{2p3/2}$ peak after sputtering can also be due to the remotion of the hydration water from the film [18]. The formation of Fe^{+3} in the outermost layers and Fe^{+3} and Fe^{+2} in the inner ones can be explained by the atmosphere oxidation of the sample during the transfer from the autoclave to the XPS spectrometer. Moreover the presence of Fe^{+2} is justified considering the deaerated autoclave environment can induce the growth of low valence state iron compounds.

The multi-component character of O_{1s} spectra (see Fig. 9) shows clearly the difference between anhydrous and hydrous oxides, and confirms the above postulated findings. The first peak at 530 ± 0.2 eV is typical for oxidized metals and the second one at 532 ± 0.5 eV is attributed to the corresponding hydrous forms. Furthermore it can be seen from the

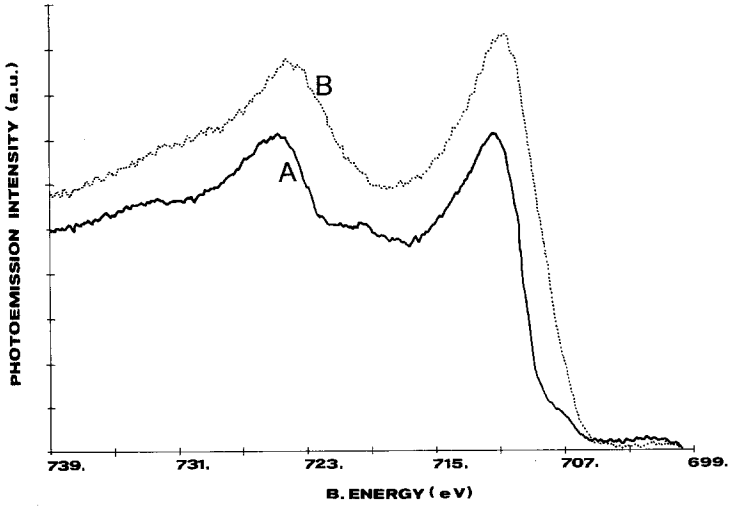

Figure 8 $Fe_{2p1/2,3/2}$ photoelectron spectra A) as received sample B) after 5 minutes of Ar^+ sputtering.

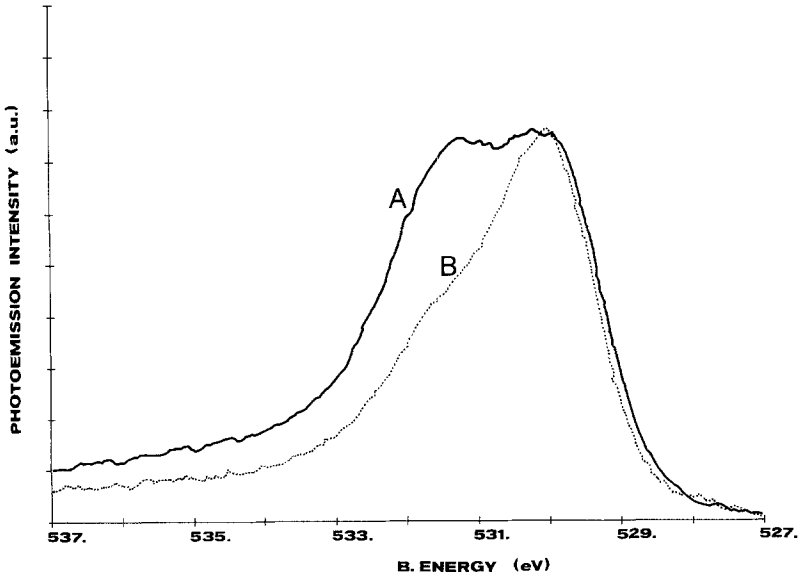

Figure 9 O_{1s} photoelectron spectra A) as received sample B) after 5 minutes of Ar^+ sputtering.

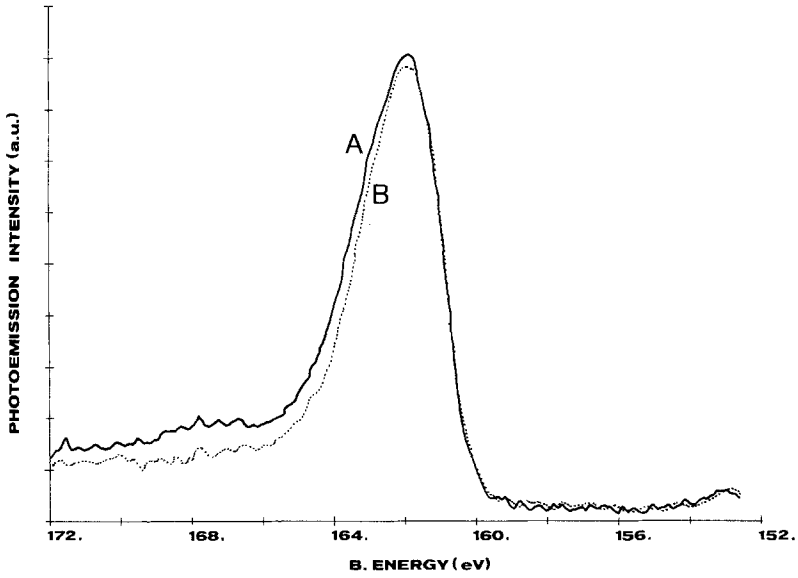

Figure 10 S_{2p} photoelectron spectra A) as received sample B) after 5 minutes of Ar^+ sputtering.

O_{1s} spectrum that the component due to the hydrous species is reduced drastically after removal of the first atomic layers. This is an artefact due to the ion bombardment [23] and exposure in ultra-high vacuum, in fact when an oxide film grows in aqueous environment a large quantity of hydrous species is expected also in the subsurface.

Concerning the nature of sulphur, the constant value of the binding energy and the unmodified line-shape of S_{2p} peak (see Fig. 10), indicate the presence of sulphides [15] both in as received and after sputtering conditions. This demonstrates that, in our case, there are no artefacts induced by ion beam degradation as observed by other authors with a much higher ion dose ($0.20\,mA\,cm^{-2}$) [25]. It is, however, difficult to recognize the nature of the sulphide as the binding energy differences between iron and chromium sulphide, metallic polysulphide, S–H bond and

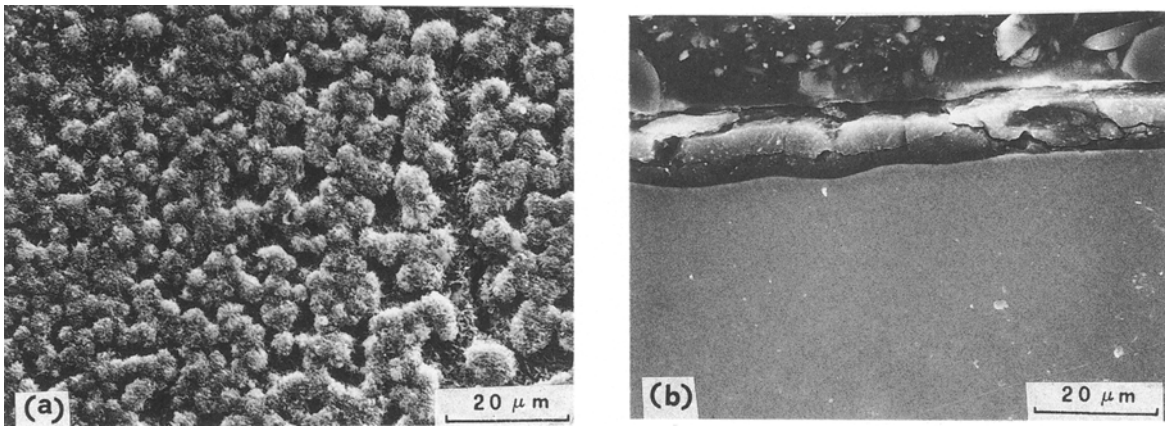

Figure 11 SEM micrograph of Test 1: surface (a) and cross section (b)

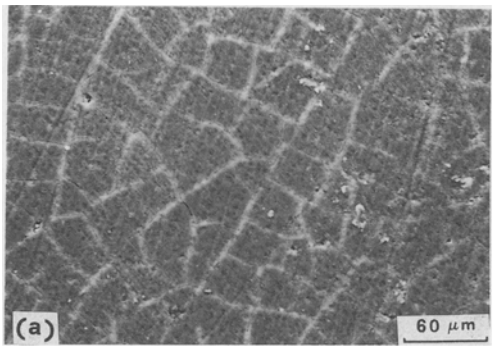

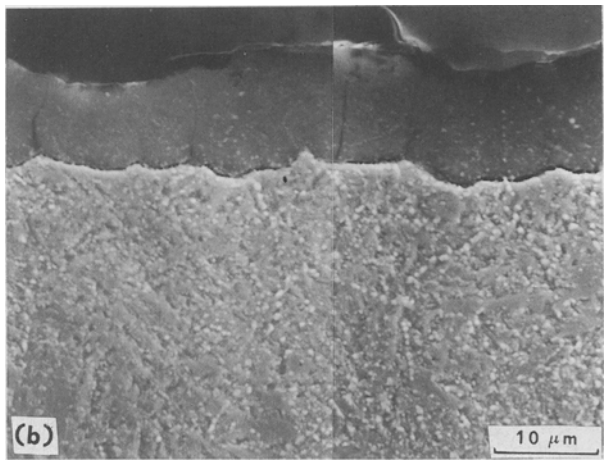

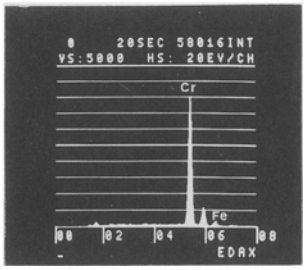

Figure 12 SEM micrograph of Test 6: surface (a) and cross section (b).

adsorbed H_2S are above the instrumental capability of XPS spectrometer [25].

XPS analysis of the film grown in most representative tests (Fig. 1–5) clearly shows that when the test solution is saturated with H_2S there is a high iron-oxide sulphide and a low chromium-oxide content (Test 1). On the contrary, the presence of CO_2 promotes the growth of chromium-oxide rich film with a low iron oxide sulphide content (Test 10).

Morphological aspects of the films were evaluated by Scanning Electron Microscopy (SEM + EDS). The most representative results are reported in Fig. 11–15, where it is evident that films grown in different conditions have different morphologies.

The mean (on 5 samples) corrosion rates (C.R.) reported in Table II, indicate that the highest values are obtai· ed with the specimens exposed to solutions saturated with H_2S (Tests 1–2) while the presence of CO_2 has an inhibiting corrosion effect (Tests 5–10). Furthermore corrosion rates measured on specimens exposed to a solution acidified to pH = 2.7 with acetic acid are generally an order of magnitude higher than those obtained for specimens exposed to a solution acidified to pH = 4.8. This pH effect is well known [3, 9, 26, 27].

To better evaluate the influence of pH_2S and pCO_2 on corrosion rates, it is useful to introduce an environmental parameter E_{H_2S,CO_2} (see Table III), representative of 13Cr steel corrosion behaviour, defined as:

$$E_{H_2S,CO_2} = pCO_2\,(pCO_2 + pH_2S)^{-1} \qquad (1)$$

The corrosion rates given in Table II are reported in Fig. 16 as a function of this environmental parameter and it is evident that corrosion rates decrease progressively with increasing CO_2 content.

On the basis of XPS results an index of protectiveness I_p, for solutions acidified to pH = 2.7, has been proposed. This index is defined by:

$$I_p = Cr^{3+}\,(Cr^{3+} + Fe^{ox})^{-1} \qquad (2)$$

In computing I_p values, the Cr^{3+} and Fe^{ox} (sulphide and oxide) atomic percentages obtained after 5 min of sputtering have been chosen to avoid interference from carbon.

The I_p index can be correlated with the environmental parameter E_{H_2S,CO_2}, and the relationship obtained is shown in Fig. 17.

Moreover, a correlation between I_p index and corrosion rate values can be proposed, which gives a clear

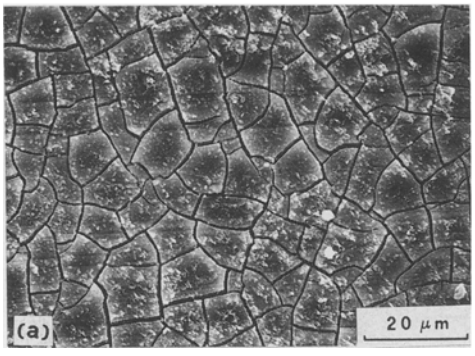

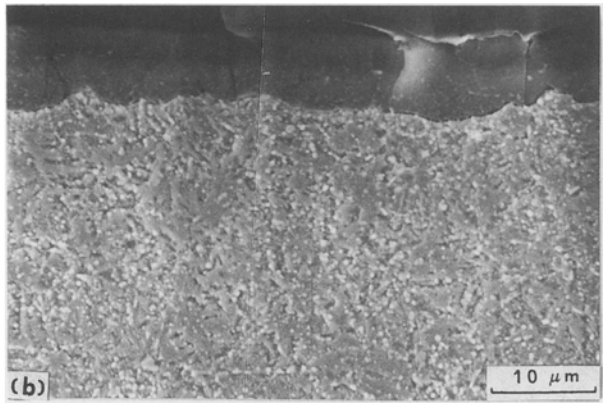

Figure 13 SEM micrograph of Test 8: surface (a) and cross section (b).

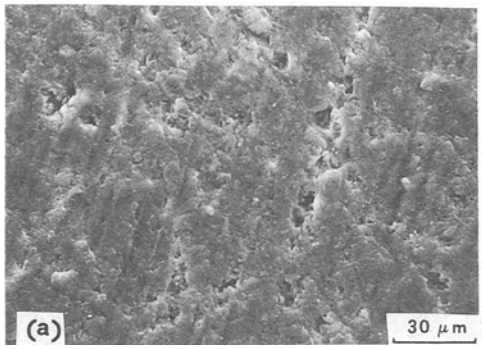

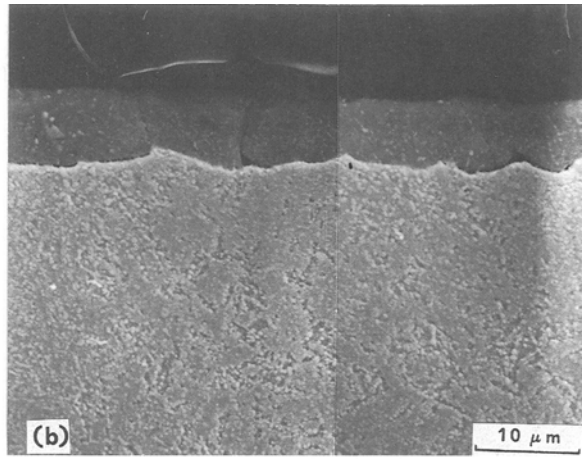

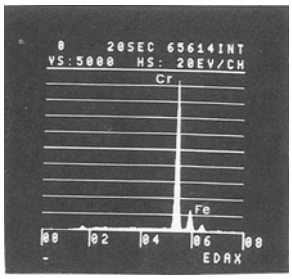

Figure 14 SEM micrograph of Test 9: surface (a) and cross section (b).

explanation of the corrosion behaviour on the basis of surface chemical composition (see Fig. 18). In fact, low corrosion rates are observed when chromium oxide enrichment occurs in the film and the I_p value is high. On the contrary, when a high amount of Fe–oxide and Fe–sulphide are present in the film, poor protection is achieved and the I_p index is low.

Surface iron enrichment, as revealed by XPS analysis, can be explained either by assuming iron precipitation during autoclave cooling, or by direct growth of the film during exposure. On the basis of the corrosion mechanisms in play, the latter mechanism is supported by the morphology of the iron-rich corrosion film as observed by SEM.

XPS and SEM analysis (see Fig. 1, 2, 11) of the films grown only in H_2S saturated conditions (Test 1 and 3), show that there is an iron and sulphur enrichment and a very low chromium oxide content.

On the contrary XPS analysis of the film grown in Test 10, carried out in a solution saturated only with CO_2, shows that chromium oxide is largely prevailing over iron in the first layers (see Fig. 5). Fig. 15 illustrates the SEM micrographs of the corresponding surface and cross section. The density and the good adhesion to the substrate of the film should be noted.

In a complex environment where both H_2S and CO_2 are present, corrosion behaviour is intermediate as a consequence of modification of chemical film composition. XPS analysis of the film grown in Test 8 (Fig. 4) reveals the simultaneous presence of Cr–oxide, Fe–oxide and Fe–sulphide; micrographs of the surface and the cross section are shown in Fig. 13. A comparison between SEM micrographs of this film with those of Test 10 (Figs. 13 and 15) indicates that the former is less compact and less adherent than the latter.

XPS results suggest that a thick hydrous chromium oxide layer is grown on stainless steel by dissolution of the alloy followed by a preferential precipitation of chromium oxide, instead of chromium sulphide. In fact $Cr_2O_3 \cdot nH_2O$ is more stable at low pH than iron oxides and iron–chromium sulphides. Nevertheless, iron may occur in this film as revealed by XPS analysis. The presence of iron and sulphur decreases film adhesion and density, with consequent lowering of corrosion resistance. It is reasonable to consider the sulphur to be responsible for this loss of stability and permeability of the corrosion film, due to the formation of sulphides in the mixed Cr–Fe–oxide film.

Some authors explained the inhibiting Co_2 effect by suggesting the formation of iron and chromium carbonates [12]. However, in our experimental conditions, XPS analysis has not revealed the presence of carbonates in the corrosion film, but has revealed iron sulphides and Fe–Cr oxides with an enrichment of Cr_2O_3 as the partial pressure of CO_2 increases. It is thus deduced that the CO_2 acts mainly on the chromium oxide formation. Schmitt has proposed a catalytic effect of the CO_2 in favouring Fe oxidation [10], thus explaining the high corrosion rates of carbon steels in CO_2-systems. When Fe-high Cr alloys are tested, the CO_2 can be similarly assumed to catalyse Cr oxidation preferentially, with subsequent formation of a protective Cr–oxide rich layer. The described corrosion mechanisms in complex H_2S–CO_2–Cl^- systems, related to chemical and morphological

TABLE III Experimental environmental parameter and protectiveness index results in function of the test conditions

Test	$E_{H_2S,CO_2} = \frac{pCO_2}{pCO_2 + pH_2S}$	$I_p = \frac{Cr^{+3}}{Cr^{+3} + Fe^{ox}}$
1	0	0.09
2	0	0.11
3	0	0.02
4	0	0.04
5	0.9	0.14
6	0.9	0.18
7	0.5	0.10
8	0.96	0.28
9	0.96	0.29
10	1	0.74

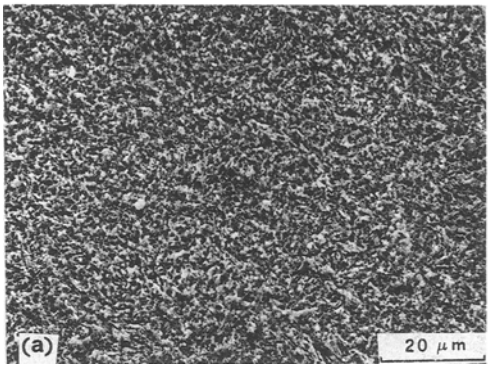

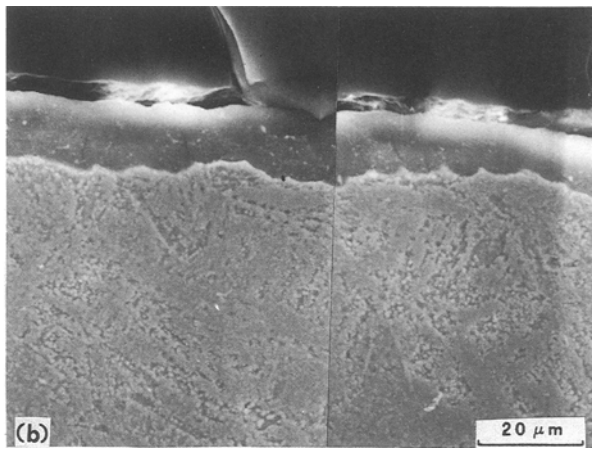

Figure 15 SEM micrograph of Test 10: surface (a) and cross section (b).

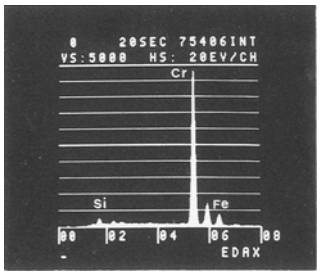

characteristics of the surface films, provide a better understanding on AISI 420 use limits. For instance, 13Cr steel can be successfully employed gas and oil wells with high pCO_2 and low pH_2S.

4. Conclusions

The complex corrosion behaviour of 13Cr–martensitic stainless steel in H_2S–CO_2–Cl^- gas and oil well environments can be explained on the basis of CO_2 and H_2S effects on the chemical composition and morphology of the corrosion films. The relatively high corrosion rate and the poor SSCC resistance of 13Cr steel in H_2S environments not containing CO_2 can be correlated with the poor protection of the Fe–oxide and Fe–sulphide films.

On the contrary, when CO_2 is also present, lower corrosion rates are observed, and its beneficial effect on SSCC resistance is verified [5]. The corrosion behaviour in this case can be explained taking into account a catalytic effect of the CO_2 in favouring a chromium oxide rich and compact film.

XPS analysis has clarified the nature of the corrosion films formed in different CO_2–H_2S–Cl^- environments, in terms of chemical composition and chemical states of iron, chromium, sulphur and carbon. The following conclusions were drawn:

(i) Corrosion rates indicated the detrimental effect of H_2S, while 13Cr steel is highly resistant to CO_2-induced corrosion. An environmental parameter E_{H_2S,CO_2} was introduced:

$$E_{H_2S,CO_2} = pH_2S\,(pH_2S + pCO_2)^{-1}$$

and good correlation has been found between E_{H_2S,CO_2} and the corrosion rates.

(ii) The XPS investigation performed on corrosion films demonstrated that the presence of H_2S favours the formation of Fe–oxide and Fe–sulphide rich films, with a poor corrosion protection. SEM analysis showed, moreover, that these films have poor adhesion and are not dense. On the contrary the

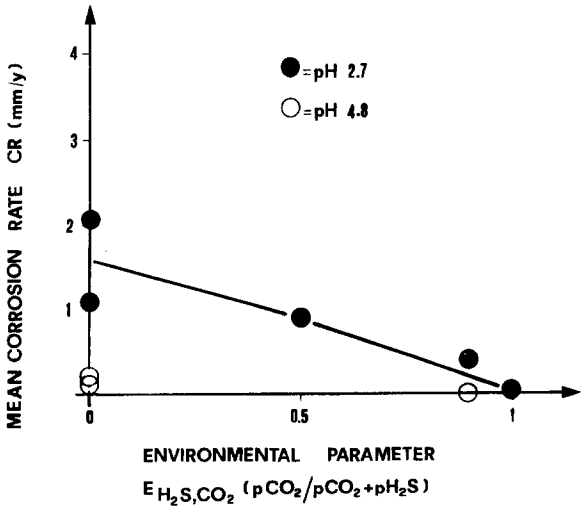

Figure 16 Mean Corrosion Rate (CR) behaviour *vs* the Environmental Parameter E_{H_2S,CO_2}.

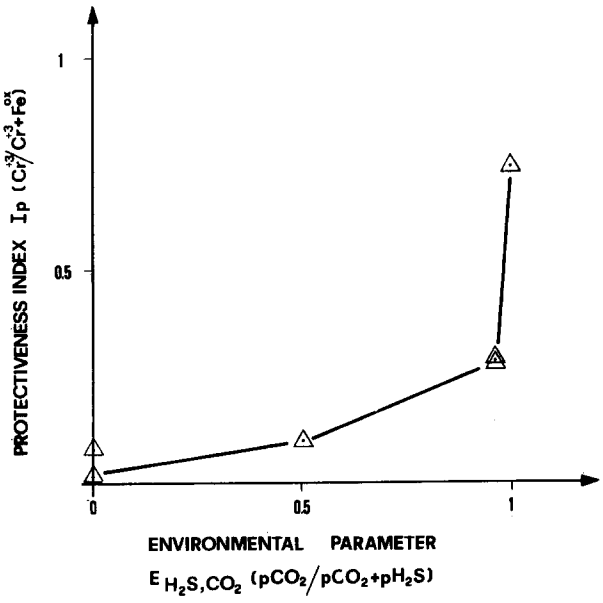

Figure 17 Protectiveness Index I_p behaviour *vs* the Environmental Parameter E_{H_2S,CO_2}.

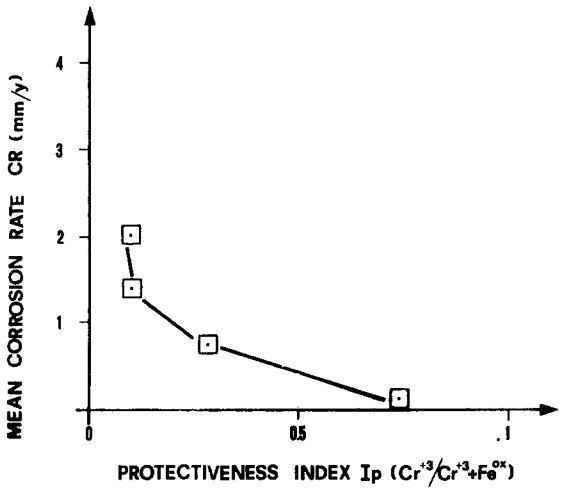

Figure 18 Mean Corrosion Rates (CR) behaviour versus the Protectiveness Index I_p.

presence of CO_2 favours the Cr–oxide enrichment in the outermost layers of the film. The Cr-rich film is very compact and protective.

(iii) A new index of film protectiveness $I_p = Cr^{3+}(Cr^{3+} + Fe^{ox})^{-1}$ was proposed on the basis of the XPS results. Correlation between this index and corrosion rates is good.

References

1. J. D. COMBES, J. G. KERR, L. J. KLEIN, *Petroleum Engineer International,* March (1983) 50.
2. J. MURAL, *Oil Gas J.* **9** 98, **23** 66, **6** 57 (1984).
3. T. MURATA, "A Criterion for Evalution and Prediction of the Sour Resistance of High Alloys", in Communication of R & D Laboratories, (Nippon Steel Corporation (1984)).
4. T. MURATA and R. MATSUHASHI, in Proceedings International Corr. Forum CORROSION/84 (New Orleans, 1986) paper no. 208.
5. F. MANCIA, *Corrosion Science,* **27** (1987) 7.
6. R. D. KANE, M. WATKINS and J. B. GREER, *Corrosion* **33** (1977) 231.
7. A. IKEDA, S. MUKAI and M. UEDA, Proceedings International Corr. Forum CORROSION/84, (New Orleans, 1984) paper no. 289.
8. H. KURAHASHI, T. KURISU, Y. SONE, K. WADA and Y. NAKAI, Proceedings International Corr. Forum CORROSION/84, (New Orleans, 1984) paper no. 212.
9. J. KLEIN, Proceedings International Corr. Forum CORROSION/84, (New Orleans, 1984) paper no. 211.
10. G. SCHMITT, Proceedings International Corr. Forum CORROSION/83, (Anaheim, 1983) paper no. 43.
11. A. IKEDA, M. UEADA and S. MUKAI, Proceedings International Corr. Forum CORROSION/83, (Anaheim, 1983) paper no. 45.
12. A. IKEDA, M. UEADA and S. MUKAI, Proceedings International Corr. Forum CORROSION/85, (Boston, 1985) paper no. 29.
13. T. KUDO, H. MIYUKI, H. OKAMOTO, J. MURAYAMA and T. MOROISHI, Proceedings International Corr. Forum CORROSION/82, (Houston, 1982) paper no. 127.
14. P. B. V. NARAYAN, A. J. BEVOLO, C. W. CHEN and O. N. CARLSON, *J. Vac. Sci. Technol.* A **3(5)** Sept./Oct. 1985.
15. P. B. V. NARAYAN, J. W. ANDEREGG and O. N. CARLSON, *Corros.* **39** (1983) 236.
16. C. D. WAGNER, L. E. DAVIS, M. V. ZELLER, J. A. TAYLOR, R. M. RAYMOND and L. H. GALE, *Surf. Interface Anal.* **3** (1981) 211.
17. J. C. CAVER, G. K. SCHWEITZER and T. A. CARLSON, *J. Chem. Phys.* **57** (1972) 980.
18. N. S. McINTYRE, "Practical Surf. An. by Auger and X-ray Photoelectron Spectroscopy", edited by D. Briggs and M. P. Seah (Wiley, New York, 1983) Chap. 10, p. 397.
19. K. ASAMI and K. ASHIMOTO, *Corrosion Science* **17** (1977) 559.
20. N. S. McINTYRE and D. G. ZETARUK, *Anal. Chem.* **49** (1977) 1521.
21. G. C. ALLEN, M. T. CURTIS, A. J. HOOPER and P. M. TUCKER, *J. Chem. Soc.* Dalton (1976) 1526.
22. C. R. BRUNDLE, T. J. CHAUNG and K. WANDELT, *Surf. Sci.* **68** (1977) 459.
23. T. J. CHAUNG, C. R. BRUNDLE and K. WANDELT, *J. Vac. Sci. Technology* **16** (1979) 797.
24. G. J. COYLE, T. TSANG and I. ADLER, *Journal of Electron Spectroscopy and Related Phenomena* **20** (1980) 169.
25. C. D. WAGNER, W. M. RIGGS, L. E. DAVIS, J. F. MOULDER and G. E. MUILENBERG, "Handbook of X-ray Photoelectron Spectroscopy", edited by G. E. Muilenberg (Perkin-Elmer Corporation, Eder Prairie, MN, 1979).
26. K. MASAMURA, S. HASHIZUME, J. SAKAY, T. ONO and I. MATSUSHIMA, Proceedings International Corr. Forum CORROSION/84, (New Orleans, 1984) paper no. 292.
27. G. FIERREO, F. M. INGO and F. MANCIA, Proceedings International. Corr. Forum CORROSION/88, (St. Louis, 1988), paper no. 215.

Received 21 December 1988
and accepted 26 April 1989